ChemComm

Ratiometric analysis of reversible thia-Michael reactions using nitrile-tagged molecules by Raman microscopy

Journal:	*ChemComm*
Manuscript ID	CC-COM-10-2023-005015.R1
Article Type:	Communication

COMMUNICATION

Ratiometric analysis of reversible thia-Michael reactions using nitrile-tagged molecules by Raman microscopy

Received 00th January 20xx,
Accepted 00th January 20xx

DOI: 10.1039/x0xx00000x

Hiroyuki Yamakoshi,*[a] Daiki Shibata,[a] Kazuki Bando,[b,c] Shinji Kajimoto,[a,d] Aki Kohyama,[a] Syusuke Egoshi,[e,f] Kosuke Dodo,[e,f] Yoshiharu Iwabuchi,[a] Mikiko Sodeoka,[e,f] Katsumasa Fujita,[b,c,g] and Takakazu Nakabayashi[a]

Ratiometric Raman analysis of reversible thia-Michael reactions was achieved using α-cyanoacrylic acid (αCNA) derivatives. Among αCNAs, the smallest derivative, ThioRas (molecular weight: 167 g/mol), and its glutathione adduct were simultaneously detected in various subcellular locations using Raman microscopy.

Raman spectroscopy is a powerful technique for visualizing small molecules.[1] The detection of Raman scattered light using Raman microscopy enables the acquisition of varied molecular information without any labeling. However, a major drawback is the difficulty in detecting specific molecules in cells owing to the overlapping of Raman signals from various intracellular molecules. Raman tags, such as alkynes and nitriles with characteristic peaks in the cellular silent region, overcome this limitation.[2–5] To date, applications of Raman tags have been limited to molecular localization analysis, and the potential applicability of obtaining structural information and monitoring dynamic chemical equilibrium states has scarcely been explored.[6–18] In 2014, we performed structure-based Raman imaging to simultaneously visualize ionic and molecular forms of a bioactive small molecule, an uncoupler carbonyl cyanide *p*-trifluoromethoxyphenylhydrazone (FCCP), for the first time in live cells[19]. Based on this precedent, we aimed to apply Raman tags to analyze the dynamic chemical equilibria of small molecules formed via covalent bonds in live cells.

In this study, we analyzed reversible thia-Michael reactions involving the formation of covalent bonds between Raman-tagged molecules and thiols using Raman microscopy. The development of techniques for the detection of thiol adducts resulting from reversible thia-Michael reactions holds paramount importance within the realm of drug development, particularly in scenarios where the cysteine residues within active sites serve as the primary target. For certain types of thiol-reactive functional groups, the propensity for swift reverse reactions prevents their thiol-adduct isolation, emphasizing the necessity of *in-situ* adduct monitoring. One such group is the α-cyanoacrylic acid (αCNA) derivatives, which undergo immediate and reversible reactions with various intracellular thiols (Fig. 1).[20,21] We hypothesized that reactions between αCNA and various thiols could be analyzed by Raman spectroscopy. The thia-Michael reaction of αCNA with thiols yields an adduct with an alkyl nitrile. Alkenyl nitriles typically show a Raman shift at lower wavenumbers (~2230 cm^{-1}) than alkyl nitriles (~2250 cm^{-1}).[3] These well-separated nitrile signals are suitable for ratiometric analysis via Raman microscopy. Any structure can be introduced as substituent R. Small substituents allow for the development of water-soluble molecules, which can be used as Raman probes for detecting thiols under cellular conditions.

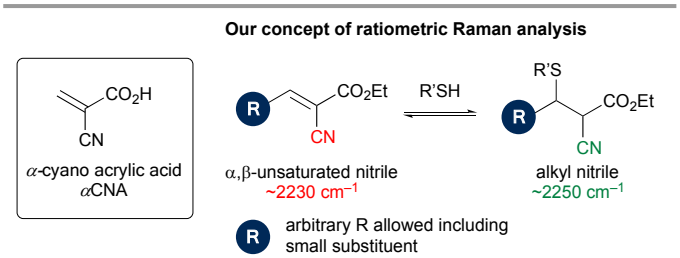

Figure 1. The reversible thia-Michael reactions of α-cyanoacrylic acid (αCNA) derivatives and thiols.

[a] *Graduate School of Pharmaceutical Sciences, Tohoku University, 6-3 Aoba, Aramaki, Aoba-ku, Sendai, 980-8578, Japan. E-mail: hiroyuki.yamakoshi.e1@tohoku.ac.jp*
[b] *Department of Applied Physics, Osaka University, 2-1 Yamadaoka, Suita, Osaka 565-0871, Japan.*
[c] *National Institute of Advanced Industrial Science and Technology (AIST), 2-1 Yamadaoka, Suita, Osaka 565-0871, Japan.*
[d] *JST PREST, 4-1-8 Honcho, Kawaguchi, Saitama 332-0012, Japan.*
[e] *Synthetic Organic Chemistry Laboratory, RIKEN Cluster for Pioneering Research, 2-1 Hirosawa, Wako, Saitama 351-0198, Japan.*
[f] *Catalysis and Integrated Research Group, RIKEN Center for Sustainable Resource Science, 2-1 Hirosawa, Wako, Saitama 351-0198, Japan.*
[g] *Institute for Open and Transdisciplinary Research Initiatives, Osaka University, 2-1 Yamadaoka, Suita, Osaka 565-0871, Japan.*
† *Electronic supplementary information (ESI) available; see DOI: 10.1039/x0xx00000x*

Intracellular thiols, such as GSH, are crucial for maintaining cellular redox homeostasis.[22]

First, we confirmed that the Raman peaks of alkenyl nitrile **1a** and alkyl nitrile **2** were separated (Fig. 2a). We selected alkenyl nitrile **1a** because its reversible thia-Michael reaction was subjected to ^{1}H-NMR analysis during the development of αCNA-based targeted covalent inhibitors.[20] Alkyl nitrile **2** was used instead of the unisolable thiol adduct **2'**. The Raman spectra of αCNA **1a** and alkyl nitrile **2** showed signals at 2228 and 2252 cm^{-1}, respectively. When a mixture of **1a** and **2** was used, two nitrile peaks were clearly observed, indicating the feasibility of ratiometric analysis. Different concentrations were used because the relative Raman intensity vs. 5-ethynyl-2'-deoxyuridine (RIE)[3] of **1a** was approximately 6-fold that of **2** (Fig. S1).

Next, we monitored the reversible thia-Michael reaction[23] of αCNA **1a** and β-mercaptoethanol (βME, **3a**) using Raman (Fig. 2b) and ^{1}H-NMR (Fig. 2b and S2) spectroscopy and compared the results. Thia-Michael reactions with αCNA are known to proceed in a neutral aqueous solution without the need for base catalysis.[20,24] Following Taunton's conditions,[20] the measurements were performed in a 3:1 mixture of dimethyl sulfoxide (DMSO) and phosphate-buffered saline (PBS) using αCNA **1a** and 1.1 equivalents of βME. The Raman spectra of the reaction mixture showed two nitrile peaks with broader shapes than those in DMSO. The ratio of **1a** to **4aa** was determined to be 17:83 based on the peak area and RIE values, which was consistent with our ^{1}H-NMR results (**1a**:**4aa** ratio = 14:86). After 30 min, the ratio did not change, indicating that the thia-Michael reaction reached equilibrium within 5 min. The dilution experiments revealed a gradual equilibrium shift from **4aa** to **1a** (**1a**:**4aa** ratio = [iii] 27:73 or [iv] 44:56). The driving force behind the retro thia-Michael reaction is the resonance stabilization of αCNA (CN and aryl groups attached to sp^2 carbons) and the destabilization of the saturated product with two electron-withdrawing groups (CN and CO_2Et) on the same sp^3 carbon.[25]

Considering the success of our ratiometric analysis, we surveyed its applicability with other thiols (Fig. 3). Alkyl thiols such as mercaptopropanol (**3b**), cysteamine derivatives (**3c**, **d**), and *N*-acetyl cysteine (**3e**) showed similar ratios to **3a**, whereas thiophenol (**3f**) showed a ratio of 42:58. Thiolates derived from acidic aromatic thiols are more stable than aliphatic thiolates. Dithiothreitol (**3g**) has two SH groups; thus, adduct **4ag** was present in a high proportion (6:94). Despite the complex tripeptide structure, the biological thiol glutathione (GSH) (**3h**) showed a reaction pattern comparable to that of **3a** (19:81), indicating that αCNA consistently reacts with GSH intracellularly. When the angiotensin-converting enzyme inhibitor, captopril (**3i**), was used, the corresponding adduct was present at a lower proportion (37:63), probably because of steric hindrance.

To evaluate the substituent effects, we screened the reactivities of a series of αCNAs (Fig. 4). Similar to related experiments conducted by Anslyn's group,[24] the introduction of an electron-donating group shifted the equilibrium to the left (**1b**), and electron-deficient aryl αCNAs **1c–f** generated a larger proportion of thiol adducts **4ca–fa**. Switching the ester functionality from ethyl ester to *tert*-butyl ester had little effect on the ratio (**1g**). The reactivities of the alkyl-substituted αCNAs **1h** and **1i** were comparable to those of **1a**. The γ-unbranched αCNA **1j** was reactive, whereas the bulkier **1k** was less efficiently converted to the thia-Michael adduct **4ka** (59:41). Additionally, 1,3-dioxolane **1l** was a more reactive substrate than **1a**.

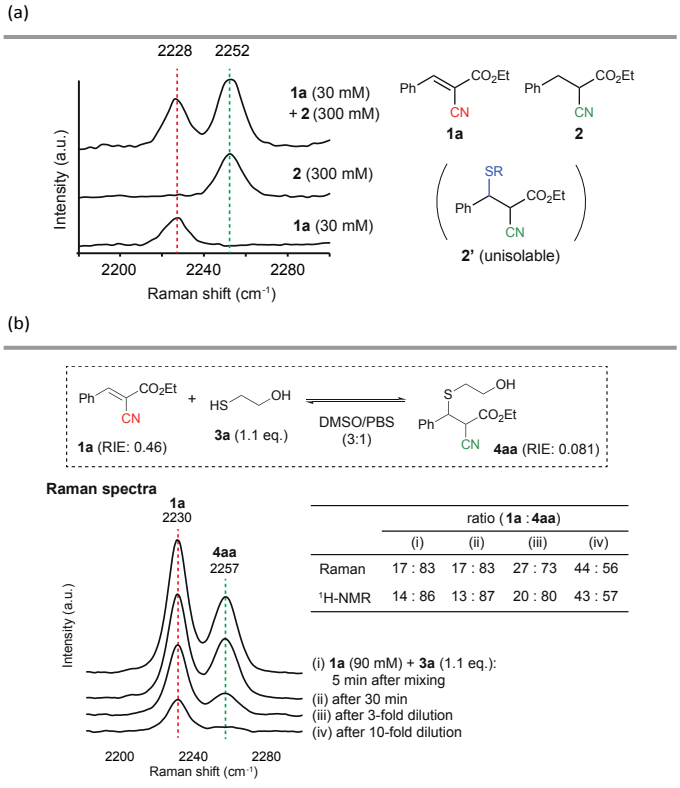

	ratio (**1a** : **4aa**)			
	(i)	(ii)	(iii)	(iv)
Raman	17 : 83	17 : 83	27 : 73	44 : 56
^{1}H-NMR	14 : 86	13 : 87	20 : 80	43 : 57

Figure 2. Ratiometric Raman analysis of the thia-Michael reaction. (a) Raman spectra of nitriles in dimethyl sulfoxide (DMSO). The dilution was performed without altering the DMSO percentage. (b) Thia-Michael reaction of **1a** with β-mercaptoethanol (**3a**) in DMSO/ PBS (3:1). Ratios were determined from the peak areas of the Raman or ^{1}H-NMR spectra (Fig. S2). a.u., arbitrary units; eq., equivalents.

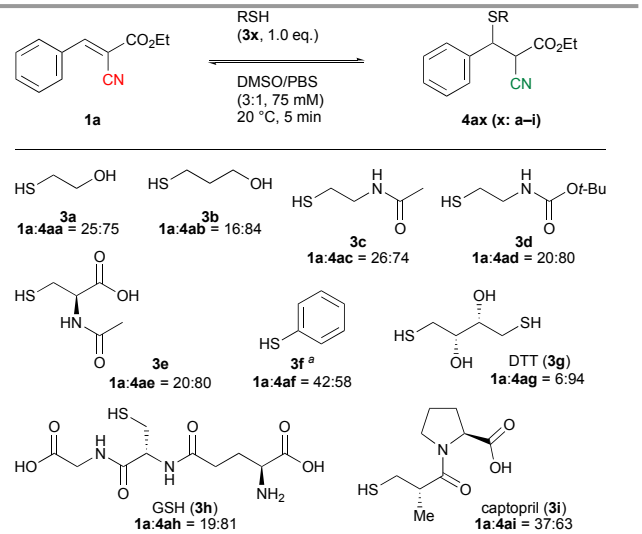

Figure 3. Thia-Michael reaction of α-cyanoacrylic acid **1a** with thiols. [a]DMSO/PBS (9:1).

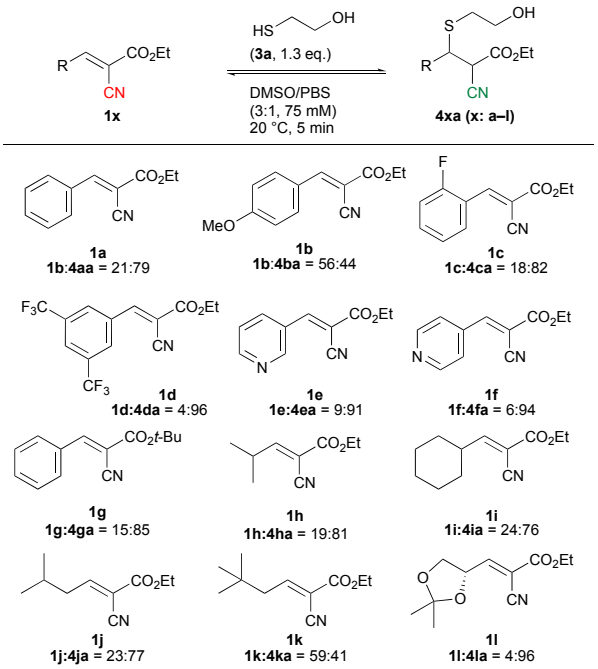

Figure 4. Thia-Michael reaction of α-cyanoacrylic acid derivatives with β-mercaptoethanol.

However, the reason for this outcome remained unclear. Thus, various αCNAs were as reactive as **1a**, except for those with electron-rich aromatic rings or bulky substituents.

Among the synthesized αCNAs, the alkyl αCNA **1h** (ThioRas: a thiol-detecting Raman sensor) is attractive because of its high reactivity with thiols and water solubility (Fig. S3 and S4). The turbidity evaluations revealed that even at 10 mM, ThioRas was almost completely dissolved in PBS, whereas the phenyl-substituted **1a** precipitated at concentrations less than 1 mM. Notably, 1,3-dioxolane **1l** was more water soluble; however, it was unstable under physiological conditions. When we examined the thia-Michael reaction of ThioRas and GSH in cell lysates (Fig. S5), the reaction readily yielded the GSH adduct, and ratiometric detection was successful even in the presence of cellular components. After adding the thiol scavenger *N*-ethylmaleimide, the GSH adduct was gradually converted to ThioRas, confirming the reaction reversibility.

Next, we performed the Raman imaging of HeLa cells treated with 600 μM **1a** and 8 mM ThioRas[§] (Fig. 5 and S6). Raman images were reconstructed according to the nitrile

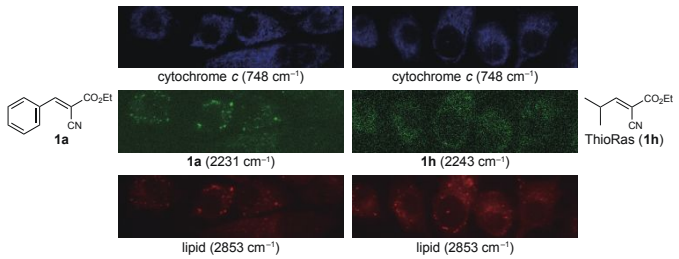

Figure 5. Raman imaging of HeLa cells treated with 600 μM **1a** or 8 mM ThioRas (**1h**). Raman images showing the distributions of **1a** at 2231 cm^{-1} (Green), **1h** at 2243 cm^{-1} (Green), cytochrome *c* at 748 cm^{-1} (Blue), and lipid at 2853 cm^{-1} (Red).

signal intensity (**1a**: 2231 cm^{-1}, and ThioRas: 2243 cm^{-1}). Compared with the granular accumulation of **1a**, ThioRas showed a more diffuse intracellular distribution with only a phenyl and isopropyl group difference. No thiol adduct peaks were detected for either compound. We speculated that the intracellular concentration of GSH may be below the detection limit. Then, ratiometric Raman analysis was performed under cellular conditions using 10 mM ThioRas with 12 mM GSH[§§]. The average Raman spectra (nitrile-wavenumber region) for each imaging area are shown in Fig. S7. After peak fitting, two nitrile peaks were successfully detected at 2232–2242 and 2255–2262 cm^{-1}, corresponding to ThioRas and its thiol adduct **4hx**, respectively. These peaks were detected within a few minutes, and no significant spectral changes occurred subsequently, suggesting that the thia-Michael reaction reached equilibrium immediately (data not shown). The RIE values for ThioRas and the thiol adduct **4hx** were 0.18 and 0.081 (Fig. S1: RIE value of alkyl nitrile **2**), respectively; their concentrations and ratios were estimated from the peak heights and RIE values (Fig. 6). The intracellular and medium concentrations of ThioRas were similar, except that the ThioRas concentration was approximately 10-fold higher in lipid droplets. The thiol concentration in the medium, estimated from the calibration curve (Fig. S8), was 13 mM. In contrast, the concentration of GSH in the medium was expected to be 12 mM (the treatment concentration), because the medium volume was much larger than that of the cells. Both concentrations are in good agreement. The ratio of unreacted ThioRas was higher in lipid droplets (**1h**:**4hx** = 80:20). The local cellular environment affected the equilibrium concentrations of ThioRas and **4hx**. In hydrophobic solvents, the thia-Michael reaction between ThioRas and βME did not occur (Fig. S9), confirming the effect of the surrounding environment on the reaction. The rapid excretion of the thiol adduct **4hx** from lipid droplets also affected the equilibrium. The hydrophilic nature of GSH is crucial for lipophilic drug metabolism. Similarly, **4hx** retention in lipid droplets is unfavourable.

When the ThioRas concentration was increased to 20 mM, the doubled nitrile signal intensity was observed (Figs. S7 and S10). The percentage of **4hx** increased in the medium, nucleus,

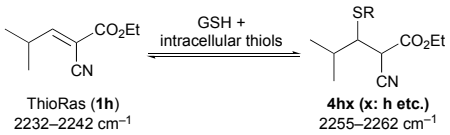

	ThioRas (**1h**) +adducts **4hx** (**1h** + **4hx**: 10 mM)			
	1h (mM)	**4hx** (mM)	**1h**:**4hx**	estimated thiol concentration (mM)
medium	3.9	6.1	42:58	13
nucleus	5.1	8.4	41:59	14
cytoplasm	5.7	8.3	42:58	13
lipid droplet	61.7	19.1	80:20	8

Figure 6. Live-cell analysis of thiols after exposure to 10 mM ThioRas in the presence of glutathione (1.2 equivalents). The concentrations of **1h** and **4hx** were calculated from the peak heights of the fitted spectra after correcting for the intensities of the RIE values. Thiol concentrations were calculated from the calibration curve (Fig. S8 and S10).

and cytoplasm with increasing GSH concentrations (Fig. S11). ThioRas allowed the successful detection of these concentration changes in cellular conditions.

ThioRas and its glutathione adduct were simultaneously detected in various subcellular locations, representing the first example of the analysis of reversible thia-Michael reactions in cellular conditions using Raman spectroscopy. To date, over 80 fluorescent thiol sensors have been developed to elucidate their biological functions.[26] However, their bulky structure (molecular weight of fluorescent dyes: >300) limits probe design. On the other hand, Raman probes do not necessarily require large sensing structures, providing greater flexibility in their size and structure (depending on their purpose) when compared to fluorescent probes. ThioRas has a molecular weight of 167 g/mol, and its isopropyl group (excluding the reactive functional groups) has a molecular weight of 43. Small sensors, which can only be realized using Raman sensors, are advantageous for detecting rapid changes in chemical equilibrium in biological studies.

Here, we used spontaneous Raman microscopy due to its general availability. With coherent microscopes (such as stimulated Raman scattering microscopes), imaging speeds can be improved.[27–33] Further studies on Raman-tag techniques will help increase the use of Raman probes as tools in the life sciences.

The authors acknowledge Dr. Menglu Li of Osaka University and AIST for technical support and helpful discussions. This research was supported in part by a Grant-in-Aid for Scientific Research (C) (JSPS KAKENHI grant number 22K06495 to H.Y.), Drug Discovery and Life Science Research [Basis for Supporting Innovative Drug Discovery and Life Science Research (BINDS)] (grant number JP22ama121040j0001 to Y.I.) from AMED, JST-CREST under Grant JPMJCR1925, the Tokyo Biochemical Research Foundation, Kowa Life Science Foundation, and Photonics Center, Osaka University, Japan.

Conflicts of interest

There are no conflicts to declare.

Notes and references

§ The maximum water-soluble concentrations were used. Note that ThioRas was completely dissolved in water at concentrations of >10 mM in the presence of GSH.

§§ Slightly higher concentrations of GSH than reported intracellular concentrations (1–10 mM) were used.[34]

1 G. Pezzotti, *J. Raman Spectrosc.*, 2021, **52**, 2348–2443.
2 H. Yamakoshi, K. Dodo, M. Okada, J. Ando, A. Palonpon, K. Fujita, S. Kawata and M. Sodeoka, *J. Am. Chem. Soc.*, 2011, **133**, 6102–6105.
3 H. Yamakoshi, K. Dodo, A. Palonpon, J. Ando, K. Fujita, S. Kawata and M. Sodeoka, *J. Am. Chem. Soc.*, 2012, **134**, 20681–20689.
4 A. F. Palonpon, J. Ando, H. Yamakoshi, K. Dodo, M. Sodeoka, S. Kawata and K. Fujita *Nat. Protoc.*, 2013, **8**, 677–692.
5 K. Dodo, K. Fujita, and M. Sodeoka, *J. Am. Chem. Soc.*, 2022, **144**, 19651‑19667.
6 H. Fujioka, J. Shou, R. Kojima, Y. Urano, Y. Ozeki and M. Kamiya, *J. Am. Chem. Soc.*, 2020, **142**, 20701–20707.
7 L. T. Wilson, W. J. Tipping, C. Wetherill, Z. Henley, K. Faulds, D. Graham, S. P. Mackay and N. C. O. Tomkinson, *Anal. Chem.*, 2021, **93**, 12786–12792.
8 X. Bi, K. Miao and L. Wei, *J. Am. Chem. Soc.*, 2022, **144**, 8504–8514.
9 H. J. Braddick, W. J. Tipping, L. T. Wilson, H. S. Jaconelli, E. K. Grant, K. Faulds, D. Graham and N. C. O. Tomkinson, *Anal. Chem.*, 2023, **95**, 5369–5376.
10 H. Fujioka, M. Kawatani, S. J. Spratt, A. Komazawa, Y. Misawa, J. Shou, T. Mizuguchi, H. Kosakamoto, R. Kojima, Y. Urano, F. Obata, Y. Ozeki and M. Kamiya, *J. Am. Chem. Soc.*, 2023, **145**, 8871–8881.
11 J. Heo, C.-K. Lim, A. Baev, A. N. Kuzmin, S. Y. Park, P. N. Prasad and S. Kim, *Dyes Pigm.*, 2016, **130**, 162–167.
12 C. Zeng, F. Hu, R. Long and W. Min, *Analyst*, 2018, **143**, 4844–4848.
13 W. J. Tipping, L. T. Wilson, S. K. Blaseio, N. C. O. Tomkinson, K. Faulds and D. Graham, *Chem. Commun.*, 2020, **56**, 14463–14466.
14 L. T. Wilson, W. J. Tipping, L. E. Jamieson, C. Wetherill, Z. Henley, K. Faulds, D. Graham, S. P. Mackay and N. C. O. Tomkinson, *Analyst*, 2020, **145**, 5289–5298.
15 S. Takemura, H. Watanabe, T. Nishihara, A. Okamoto and K. Tanabe, *RSC Adv.*, 2020, **10**, 36119–36123.
16 J. Du and L. Wei, *J. Am. Chem. Soc.*, 2022, **144**, 777–786.
17 J. Shou and Y. Ozeki, *Opt. Lett.*, 2021, **46**, 2176–2179.
18 J. Ao, X. Fang, X. Miao, J. Ling, H. Kang, S. Park, C. Wu and M. Ji, *Nat. Commun.*, 2021, **12**, 3089.
19 H. Yamakoshi, A. F. Palonpon, K. Dodo, J. Ando, S. Kawata, K. Fujita and M. Sodeoka, *Chem. Commun.*, 2014, **50**, 1341–1343.
20 I. M. Serafimova, M. A. Pufall, S. Krishnan, K. Duda, M. S. Cohen, R. L. Maglathlin, J. M. McFarland, R. M. Miller, M. Frödin and J. Taunton, *Nat. Chem. Biol.*, 2012, **8**, 471–476.
21 X. Jiang, J. Chen, A. Bajić, C. Zhang, X. Song, S. L. Carroll, Z.-L. Cai, M. Tang, M. Xue, N. Cheng, C. P. Schaaf, F. Li, K. R. MacKenzie, A. C. M. Ferreon, F. Xia, M. C. Wang, M. Maletić-Savatić and J. Wang, *Nat. Commun.*, 2017, **8**, 16087.
22 S. Raj Rai, C. Bhattacharyya, A. Sarkar, S. Chakraborty, E. Sircar, S. Dutta and R. Sengupta, *ChemistrySelect*, 2021, **6**, 4566–4590.
23 P. A. Jackson, J. C. Widen, D. A. Harki and K. M. Brummond, *J. Med. Chem.*, 2017, **60**, 839–885.
24 Y. Zhong, Y. Xu and E. V. Anslyn, *European J. Org. Chem.*, 2013, **2013**, 5017–5021.
25 E. H. Krenske, R. C. Petter and K. N. Houk, *J. Org. Chem.*, 2016, **81**, 11726–11733.
26 S. Wang, Y. Huang and X. Guan, *Molecules*, 2021, **26**, 3575.
27 N. Qian and W. Min, *Curr. Opin. Chem. Biol.*, 2022, **67**, 102115.
28 J. Du, H. Wang and L. Wei, *ACS Chem. Biol.*, 2022, **17**, 1621–1637.
29 A. Adamczyk, E. Matuszyk, B. Radwan, S. Rocchetti, S. Chlopicki and M. Baranska, *J. Med. Chem.*, 2021, **64**, 4396–4409.
30 S. Bakthavatsalam, K. Dodo and M. Sodeoka, *RSC Chem Biol*, 2021, **2**, 1415–1429.
31 J. Xu, T. Yu, C. E. Zois, J.-X. Cheng, Y. Tang, A. L. Harris and W. E. Huang, *Cancers*, 2021, **13**, 1718.
32 L. Wei, Z. Chen, L. Shi, R. Long, A. V. Anzalone, L. Zhang, F. Hu, R. Yuste, V. W. Cornish and W. Min, *Nature*, 2017, **544**, 465–470.
33 F. Hu, C. Zeng, R. Long, Y. Miao, L. Wei, Q. Xu and W. Min, *Nat. Methods*, 2018, **15**, 194–200.
34 Y. Zhu, H. Pan, Y. Song, C. Jing, J.-A. Gan and J. Zhang, *Dyes Pigm.*, 2021, **191**, 109376.

